Chapter 2

Kinetics of Chemical Reactions

In this chapter, a theoretical treatment of chemical reaction kinetics will be presented. The particular case of ion-molecule reactions, which is necessary for a complete comprehension and interpretation of the experimental results presented in chapter 5, will be discussed in detail.

2.1 Basic Concepts of Reaction Kinetics

For the theoretical treatment of chemical reactions in the gas-phase, it is necessary to establish the basic definitions of the reaction kinetics.[20–22] For the case that two species, A and B react and produce the species, C and D, one can write:

$$aA + bB \longrightarrow cC + dD \tag{2.1}$$

where a, b, c and d represent the stoichiometric coefficients, giving the number of moles of the respective reactant and product participating in the reaction. A chemical reaction is described by the *rate of reaction* R, which is directly proportional to the change in the concentration of a chemical species taking part in the reaction as a function of time. The rate of reaction R is defined as:

$$R = -\frac{1}{a}\frac{d[A]}{dt} = -\frac{1}{b}\frac{d[B]}{dt} = \frac{1}{c}\frac{d[C]}{dt} = \frac{1}{d}\frac{d[D]}{dt} \tag{2.2}$$

where $[X]$ is the concentration of the species X. Although the SI unit for the rate of reaction is $mol/(dm^3 s)$, the unit $molecules/(cm^3 s)$ is commonly used for chemical

reactions in the gas-phase. The reaction rate expression can be written as:

$$R = k[A]^m[B]^n \tag{2.3}$$

where k is the *rate coefficient* or *rate constant*, while m and n represent the *order of reaction* with respect to reactant A and B.

Chemical reactions can have different orders. For example, there are first-order reactions or *unimolecular reactions* (A$\longrightarrow$ products), second-order or *bimolecular reactions* (A + B $\longrightarrow$ products), third-order or *termolecular reactions* (A + B + C $\longrightarrow$ products) etc. Elementary chemical reactions with higher orders than three (four, five, etc.) are theoretically possible but have not been found to take place in nature, since the collision of more than three particles at once is highly improbable.

In the case of a first-order reaction, the reaction rate has the following form:

$$R = k[A] = -\frac{d[A]}{dt} \tag{2.4}$$

Through integration of equation 2.4 with respect to the time t, an expression for the concentration $[A]$ can be obtained:

$$\int \frac{d[A]}{[A]} = -\int k dt \tag{2.5}$$

$$[A]_t = [A]_0 \cdot e^{-kt} \tag{2.6}$$

where $[A]_0$ is the initial concentration of the reactant A and $[A]_t$ represents the concentration after the reaction time t. Commonly, the rate coefficient k can be determined experimentally. In conformity with equation 2.6, the value for k can be extracted by fitting the experimental values of the concentration $[A]$, measured as a function of reaction time t.[23–27]

In the case of a second and third-order reaction, the reaction rates have the expressions:

$$R = \frac{d[A]}{dt} = -k[A][B] \tag{2.7}$$

and

$$R = \frac{d[A]}{dt} = -k[A][B][C] \tag{2.8}$$

respectively. With increasing reaction order, the differential equation (*rate law expression*) becomes more complicated. When analytical solutions are difficult to find through direct integration of the reaction rate equations, the *pseudo-first-order approximation method* can be used. The rate constant k, which appears in equation 2.7, is a bimolecular constant and will be denoted with $k^{(2)}$, where the upper index in parenthesis represents the order of the reaction. If $[A] \gg [B]$ and $[A]$ can therefore be assumed to remain constant during the reaction, then equation 2.7 can be written as:

$$\frac{d[A]}{dt} = -k^{(2)}[A][B] = -k^{(1)}[B] \tag{2.9}$$

with

$$k^{(1)} = k^{(2)}[A] \tag{2.10}$$

where $k^{(1)}$ is the pseudo-first-order rate coefficient. With this approximation the second-order reaction becomes pseudo-first-order and follows the kinetics of a first-order reaction.

Usually, most chemical processes are more complicated than those discussed previously and involve many elementary steps. An important example is the scheme of first-order consecutive reactions involving a reversible step which is described by:

$$A \leftrightarrows B \qquad k_1,\ k_{-1} \tag{2.11}$$

$$B \rightarrow C \qquad k_2 \tag{2.12}$$

This type of reaction is significant for the interpretation of the experimental results shown in chapter 5 and a detailed description will be presented in section 2.2.2. The rate law expressions for this consecutive reaction have the following form:

$$\frac{d[A]}{dt} = -k_1[A] + k_{-1}[B] \tag{2.13}$$

$$\frac{d[B]}{dt} = k_1[A] - k_{-1}[B] - k_2[B] \tag{2.14}$$

$$\frac{d[C]}{dt} = k_2[B] \tag{2.15}$$

An explicit analytical solution for this system of differential equations is difficult to obtain. In order to simplify the problem, the *steady-state approximation* can be

employed. This approximation assumes that the concentration of the intermediate product is small and changes very slowly in time ($d[X]/dt \cong 0$). Applying the steady-state approximation to the intermediate product $[B]$ implies:

$$\frac{d[B]}{dt} \cong 0 \tag{2.16}$$

and equation 2.14 becomes:

$$k_1[A] - k_{-1}[B]_{ss} - k_2[B]_{ss} = 0 \tag{2.17}$$

where $[B]_{ss}$ is the steady state concentration of the intermediate product. If this expression is introduced in the equations 2.13 - 2.15, a simplified set of differential equations is obtained:

$$\frac{d[A]}{dt} = -\frac{k_1 k_2}{k_{-1} + k_2}[A] \tag{2.18}$$

$$[B]_{ss} = -\frac{k_1}{k_{-1} + k_2}[A] \tag{2.19}$$

$$\frac{d[C]}{dt} = \frac{k_1 k_2}{k_{-1} + k_2}[A] \tag{2.20}$$

In such complex consecutive reactions, the rate coefficient of one of the elementary steps can influence the overall reaction rate in a decisive way and it is then referred to as the *rate-determining step*. For example, when $k_2 \gg k_{-1}$ in the reaction presented above, the intermediate product B is transformed to C much faster than it decays back to A and the rate-determining step is the formation of the intermediate product B with the rate-determining coefficient k_1.

The rate coefficients not only depend on the concentration of the reaction educts but also show a pronounced dependence on the reaction temperature. J. H. van't Hoff in 1884[28] and S. Arrhenius in 1889[29] established an empirical relation for the temperature dependence of the reaction rate. This expression is referred to as the *Arrhenius law* and has the following form:

$$k(T) = A \ \exp\left(-\frac{E_a}{k_B T}\right) \tag{2.21}$$

where E_a represents the activation energy, A represents the pre-exponential factor, k_B denotes the Boltzmann constant and T denotes the temperature. The activation energy E_a is defined as the energy barrier on the potential energy surface which the

reactants have to overcome in order to form the reaction products. According to the Arrhenius equation, $k(T)$ increases with increasing temperature, *i.e.* the chemical reaction proceeds faster with increasing temperature. However, there are chemical reactions which show a non-Arrhenius temperature dependence. This usually occurs when the chemical process involves the formation of an energetically excited intermediate product which undergoes collisions with the surrounding molecules in order to be stabilized and thus, the measured reaction is not a single elementary step but contains a number of different intermediate steps. An example of non-Arrhenius temperature dependence will be presented in the next section.

2.2 Ion-Molecule Reactions

The chemical reactions of ions with molecules were intensively studied during the last century. It is assumed that this type of reactions plays an important role in the synthesis of large molecules inside interstellar clouds.[30] Furthermore, the understanding of gas discharges and plasma also involve the study of ion-molecule reactions.[31] Together with the appearance of cluster science, the question of size selective chemistry was raised since the physical and chemical properties of the clusters show a pronounced size dependence. It was shown that the charge of the clusters is an essential parameter for enabling chemical reactions by changing the bond length of an adsorbed molecule.[25,32–35] Therefore, the field of ion-molecule reactions represents an important issue for the interpretation of the experimental results presented in chapter 5.

In this section, the theoretical treatment of ion-molecule reactions will be presented. First, the Langevin theory will be discussed. After this, the Lindemann mechanism will be described and the statistical theories of Rice-Ramsperger-Kassel (RRK) and Rice-Ramsperger-Kassel-Marcus (RRKM) will be outlined.

2.2.1 Langevin Theory

A simplified approach for describing chemical reactions is the "*hard-sphere collision model*", which considers a chemical reaction as a collision of rigid spheres and does not take into account any other intrinsic information about the reactants. In this case, the reaction cross section, σ is given by:

$$\sigma = \pi d^{\,2} = \pi(r_A + r_B)^2 \tag{2.22}$$

where $d = r_A + r_B$ is the sum of the radii of the molecules A and B. This model assumes that the probability of a chemical reaction to occur between molecule A and B is 1 ($P_{AB} = 1$) when the distance between the molecules is $r_{AB} \leq d$ and the probability for a reaction is 0 ($P_{AB} = 0$) when $r_{AB} > d$.

The reaction rate, $k(T)$ for the hard sphere collision model is defined as:

$$k(T) = \int v\sigma f(v)dv \tag{2.23}$$

where v represents the relative velocity of the molecules A and B ($v = |v_A - v_B|$) and $f(v)$ is the distribution function of velocities. Introducing relation 2.22 in equation 2.23 and taking into account that the molecules have a Maxwell-Boltzmann distribution of velocities, the equation 2.23 becomes:

$$k(T) = \sqrt{\frac{8\pi k_B T}{\mu}}\; d^2 \tag{2.24}$$

where k_B denotes the Boltzmann constant, T represents the temperature and μ represents the reduced mass of the molecules A and B:

$$\mu = \frac{m_A m_B}{m_A + m_B} \tag{2.25}$$

By using the expression 2.24, the collision rate coefficient can be calculated for a given temperature and pressure.

However, considering molecules as rigid spheres and neglecting all the molecular interaction potentials does not lead to an appropriate description of real chemical reactions. In comparison to other kinetic models, the values obtained from the hard-sphere collision theory overestimate the reaction rates for gas-phase reactions.

In order to obtain a better description of the collision between two molecules, a form for the molecular interaction potential should be assumed. Usually, a Lennard-Jones potential is employed which contains an attractive van der Waals term ($\sim r^{-6}$) and an empirical repulsive part ($\sim r^{-12}$) that dominates the short-range molecular interactions.[20] The first theory of ion-molecule reactions was proposed by P. Langevin in 1905.[36] The *Langevin theory* describes the interaction between an ion and a non-polar molecule. According to this, the effective interaction potential is given by the following expression:

$$V(r) = U(r) + \frac{L^2}{2\mu r^2} = -\frac{1}{2}\,\frac{\alpha\, e^2}{r^4} + \frac{L^2}{2\mu r^2} \tag{2.26}$$

where α represents the polarizability of the neutral molecule, e denotes the elementary charge, r represents the relative distance between the ion and the molecule and L represents the classical angular momentum. The angular momentum has the form $L = \mu v b$, with v as the relative velocity of the two particles and b as the impact parameter. The second term in expression 2.26 describes the repulsion between the two particles and is referred to as the centrifugal term. The relation 2.26 can be written in terms of the kinetic energy $E = 1/2\mu v^2$ and in this case, the effective potential becomes:

$$V(r) = -\frac{1}{2}\,\frac{\alpha e^2}{r^4} + E\left(\frac{b}{r}\right)^2 \tag{2.27}$$

Fig. 2.1 shows the form of the interaction potential between an ion and a nonpolar molecule according to the Langevin theory ($V(r)$) combined with a repulsive Lennard-Jones term (ar^{-12}) which describes the nuclei repulsion ($V_L(r) = V(r) + ar^{-12}$).

The *Langevin potential* has a maximum along the reaction coordinate, that is given by:

$$V_{max} = \frac{1}{2}\,\frac{E^2 b^4}{\alpha e^2} \tag{2.28}$$

where V_{max} represents the centrifugal barrier, which has to be overcome for the chemical reaction to take place. From equation 2.28, it can be observed that the height of the centrifugal barrier is directly proportional to the value of the kinetic energy E. Thus, for $E \to 0$ the centrifugal barrier $V_{max} \to 0$. Since the mean kinetic energy of a molecular ensemble depends on the temperature ($\langle E \rangle = 3/2\ k_B T$), for $T \to 0$ the mean kinetic energy and therefore, the mean centrifugal barrier will decrease to zero.

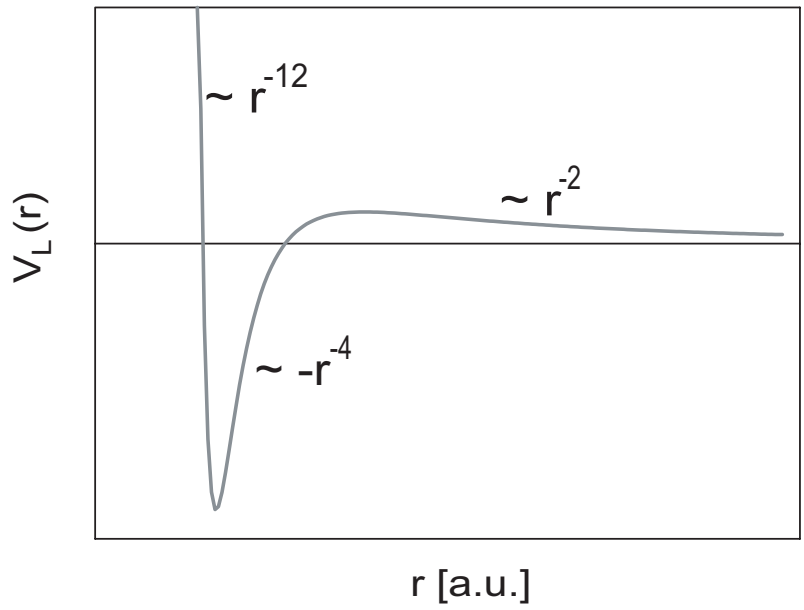

Figure 2.1: The interaction potential between an ion and a molecule according to the Langevin theory ($V(r)$), combined with a Lennard-Jones repulsive term (ar^{-12}). The interaction potential is depicted as a function of the relative intermolecular distance.

The critical impact parameter corresponding to V_{max} for which a chemical reaction takes place is:

$$b_c = \left(\frac{2\alpha e^2}{E}\right)^{1/4} \tag{2.29}$$

For impact parameter values $b \leq b_c$, the reaction probability is P = 1 while for $b > b_c$, the reaction does not occur and P = 0.

Similar to the hard-sphere collision model, the reaction cross section or the *Langevin cross section* is defined as:

$$\sigma_L = \pi b_c^2 = \pi \left(\frac{2\alpha e^2}{E}\right)^{\frac{1}{2}} \tag{2.30}$$

The rate constant for the Langevin model can be calculated as:

$$k_L = \int v\sigma(v)f(v)dv \tag{2.31}$$

If one takes into account that the molecules have a Maxwell-Boltzmann distribution of velocities and equation 2.30 is introduced into equation 2.31, the expression for the *Langevin rate constant* is obtained:

$$k_L = \sqrt{\frac{4\pi^2 \alpha e^2}{\mu}} \tag{2.32}$$

From the previous expression, one can observe that k_L depends only on the reduced mass of the molecules and the polarizability of the nonpolar molecule. No information about the structure or other chemical and physical properties of the molecules are taken into account in this model.

The Langevin theory can also be applied to the description of chemical reactions between ions and dipolar molecules. In this case, the molecular interaction potential has the form:[37,38]

$$U(r) = -\frac{1}{2}\frac{\alpha e^2}{r^4} - \frac{e\mu_D}{r^2}\ cos\theta \tag{2.33}$$

where α and μ_D represent the polarizability and the permanent dipole moment of the neutral molecule, respectively, and θ is the angle formed by the dipole and r.

Although the Langevin theory does not contain any temperature dependence, the rate constant is dependent on the reaction temperature in the case of an ion-dipole molecule reaction. T. Su, W. J. Chesnavich and M. T. Bowers modelled this type of reaction by considering the ion as a point charge and the dipolar molecule as two-dimensional rigid rotor.[37,38] They found that the ratio between the capture rate constant $k_{cap}(T)$ and the Langevin rate constant k_L depends only on two reduced parameters, T_R and I^* :

$$\frac{k_{cap}(T)}{k_L} = K(T_R, I^*) \tag{2.34}$$

where $k_{cap}(T)$ represents the rate constant for the reaction between an ion and a dipolar molecule, $T_R = 2\alpha k_B T/\mu_D^2$ and $I^* = \mu_D I/\alpha e\mu$ with I as the moment of inertia of the neutral dipolar molecule. An empirical expression was found for $K(T_R, I^*)$, which is given by:[37,38]

$$K(T_R, I^*) = 0.4767 \cdot x + 0.6200 \qquad \text{for } x \geq 2 \tag{2.35}$$

and

$$K(T_R, I^*) = \frac{(x + 0.5090)^2}{10.526} + 0.9754 \qquad \text{for } x < 2 \tag{2.36}$$

with

$$x = \frac{1}{\sqrt{T_R}} = \frac{\mu_D}{(2\alpha k_B T)^{1/2}} \tag{2.37}$$

Introducing the equations 2.35 and 2.36 in expression 2.34, the capture rate constant $k_{cap}(T)$ for the reaction between an ion and a dipolar molecule can be calculated as:

$$k_{cap}(T) = k_L \cdot (0.4767 \cdot x + 0.6200) \qquad \text{for } x \geq 2 \tag{2.38}$$

$$k_{cap}(T) = k_L \cdot \left(\frac{(x + 0.5090)^2}{10.526} + 0.9754 \right) \qquad \text{for } x < 2 \tag{2.39}$$

The equations 2.38 and 2.39 will be utilized for the modelling of the reaction between cluster ions and carbon monoxide molecules which will be presented in detail in chapter 5.

In the Langevin theory, the expression of the reaction rate constant k_L does not depend on the reaction temperature and pressure which are however essential parameters for the description of a chemical reaction. For a better understanding of the intrinsic mechanisms involved in a chemical process, other models have been developed. In the following section, the Lindemann theory, which is an important step in the understanding of unimolecular thermal reactions will be presented.

2.2.2 Lindemann Mechanism

In 1922, F. A. Lindemann proposed the model of collisionally activated thermal reactions in order to explain unimolecular decomposition reactions.[39] At that time, it was considered that the energy necessary for an unimolecular reaction to occur is provided by the radiation taken from the surrounding medium (radiation hypothesis[21]). In his model, Lindemann assumed that the activation barrier for a chemical reaction can be overcome through bimolecular collisions. According to this theory, a molecule can be energized through collisions ($B + B \leftrightarrows B^* + B$) and an intermediate product of the reaction is formed (B^*). The energized intermediate product (B^*) can be de-energized through collision with another molecule or can overcome the energy barrier and undergo an unimolecular decomposition reaction ($B^* \rightarrow Products$).

The ion-molecule reactions show a particular behavior, since they present a very small or even no activation barrier (see section 2.2.1). It was experimentally found that ion-molecule reactions have a pronounced negative temperature dependence, deviating from an Arrhenius type dependence.[40–43] This unexpected behavior can be understood by considering a Lindemann type formalism referred to as the *inverse Lindemann mechanism* or *energy transfer mechanism*.[44] According to this model, an intermediate activated molecular complex will be formed through a bimolecular collision. A subsequent collision of the intermediate activated complex with another molecule (third body) is necessary in order to stabilize the reaction product. In analogy to equations 2.11 and 2.12, this process can be formally written as:

$$A^{+/-} + M \rightleftarrows (AM^{+/-})^* \qquad k_1,\ k_{-1} \tag{2.40}$$

$$(AM^{+/-})^* + X \rightarrow AM^{+/-} + X \qquad k_2 \tag{2.41}$$

where $A^{+/-}$ represents the positive or negative ion, M denotes the reactant gas molecule and X is an inert gas molecule (third body). k_1, k_{-1} and k_2 represent the reaction rate constants for the forward, backward and stabilization reaction, respectively. Employing the steady-state approximation for the activate intermediate complex $(AM^{+/-})^*$, the expression for the overall first-order reaction rate constant is given by:

$$k^{(1)}_{overall} = \frac{k_1 k_2 [M][X]}{k_{-1} + k_2[X]} \tag{2.42}$$

If the time interval between the formation of the activated complex and the stabilization collision is long compared to the lifetime of the intermediate product $(AM^{+/-})^*$, the activated complex will decompose back to the initial reactants. Since the formation of the reaction products depends on the collision with the buffer gas molecules, the entire process is a competition between intermolecular collisional energy transfer and intramolecular rearrangement of the excess energy of the activated complex among its degrees of freedom.[a]

Two limiting cases can be distinguished as a function of the buffer gas concentration $[X]$. In the *high-pressure limit*, the stabilization process occurs much faster than the dissociation of the activated complex. In this case, $k_2[X] \gg k_{-1}$ and the

[a] The process of the intramolecular rearrangement of the excess energy is referred to as intramolecular vibrational energy redistribution (IVR).

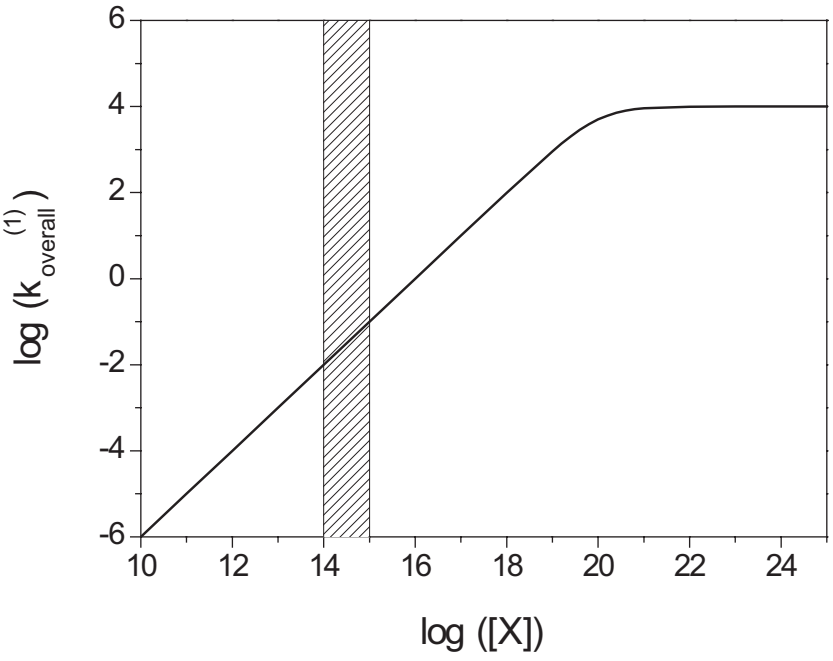

Figure 2.2: The dependence of the first-order rate constant $k^{(1)}_{overall}$ on the buffer gas pressure $[X]$ according to the Lindemann mechanism for $k_1 = k_2 = 10^{-10} cm^3 s^{-1}$, $k_{-1} = 10^{10} s^{-1}$ and $[X] = 10^{14} cm^{-3}$. The hatched area represents the working pressure range for all the experiments presented in this work.

reaction rate becomes:

$$k^{(1)}_{overall} \sim k_\infty = k_1[M] \tag{2.43}$$

From expression 2.43, it can be seen that in this regime, the reaction rate does not depend on the buffer gas pressure.

In the *low-pressure limit*, the condition $k_2[X] \ll k_{-1}$ is fulfilled and the rate determining step is represented by the collisional energy transfer to the buffer gas. The reaction rate in this case is given by:

$$k^{(1)}_{overall} \sim k_0 = \frac{k_1 k_2 [M][X]}{k_{-1}} \tag{2.44}$$

One of the most important achievements of the Lindemann theory was the proper description of the experimental finding that the order of the reaction rate constant changes from first-order in the high-pressure regime to second-order in the low-pressure limit.[45,46] The double logarithmic plot of the overall reaction rate as a

function of the buffer gas pressure according to the Lindemann mechanism is shown in Fig. 2.2, where the values $k_1 = k_2 = 10^{-10}\ cm^3 s^{-1}$, $k_{-1} = 10^{10}\ s^{-1}$ and $[X] = 10^{14}\ cm^{-3}$ are used for the calculation of $k^{(1)}_{overall}$. The hatched area represents the experimental pressure range for all the results presented in this work.

The expression for $k^{(1)}_{overall}$ can be determined when k_1, k_{-1} and k_2 are known. k_1 and k_2 can be calculated by using the Langevin collision theory. For the calculation of the dissociation rate constant k_{-1}, statistical models like RRK (Rice-Ramsperger-Kassel) theory and RRKM (Rice-Ramsperger-Kassel-Marcus) theory are used. The RRK and RRKM theories will be presented in detail in the next section.

2.2.3 RRK and RRKM Theory

In 1927-1928, O. K. Rice, H. C. Ramsperger and L. S. Kassel elaborated a statistical theory for the calculation of unimolecular dissociation rates,[47,48] known as *RRK theory*, which is based on the following assumptions:

- A molecule is considered as a collection of s coupled harmonic oscillators.
- The intramolecular distribution of the excess energy (IVR) occurs faster than the unimolecular decomposition of the activated complex back to reactants (referred to as the *"ergodic assumption"*).

The unimolecular decomposition of an activated complex occurs when an amount of energy E, higher than a critical energy E_0 ($E > E_0$) is transferred to a chosen vibrational degree of freedom, which represents the critical mode that leads to reaction. The reaction probability is given by the number of ways to arrange the excess energy in one specific oscillator, divided by the number of ways to distribute the energy E brought into the system between s oscillators. Thus, the reaction probability can be calculated by using classical mathematical combinatorial methods and the RRK rate constant has the form:

$$k(E) = \nu \left(\frac{E - E_0}{E}\right)^{s-1} \tag{2.45}$$

where ν is the frequency factor and represents the vibrational frequency of the critical oscillator which has the energy ($E > E_0$). E_0, the critical energy, can be identified

as the binding energy of the activated complex. In order to obtain a good agreement between experiment and theory, a smaller value $s_{eff} < s$ for the total number of the vibrational degrees of freedom should be considered in the *classical RRK theory* and this is mainly due to the classical treatment of the degrees of freedom.[49] In 1928, L. S. Kassel developed a quantum mechanical approach of the RRK theory, referred to as the *quantum RRK theory*.[50] This model considers that the molecular energies involved in the chemical process contain a specific number of energy quanta. Although the quantum RRK theory is an improvement of the classical version, the assumption of s identical oscillators with the same frequency still leads to some discrepancies between experiment and theory. Despite this, the RRK theory can be successfully applied to the estimation of the binding energy of different molecular complexes, as will be shown in chapter 5.

The *Rice-Ramsperger-Kassel-Marcus theory* (RRKM) was developed by R. A. Marcus and is based on the RRK theory.[51] The RRKM model takes into account the vibrational and rotational energies of the molecule and uses the transition state concept. As in the RRK theory, the ergodic assumption is made and the RRKM theory can also be described as a microcanonical transition state theory.

The most general expression for the RRKM reaction rate constant is given by:

$$k(E) = \frac{1}{h} \frac{G(E^{\ddagger})}{N(E_v)} \tag{2.46}$$

where $G(E^{\ddagger})$ represents the sum of states for the active degrees of freedom[b] in the transition state and $N(E_v)$ denotes the density of states for the active degrees of freedom in the reactant. For the calculation of the RRKM reaction rate constant, the classical expressions for the sum and density of states can be used:

$$G(E) = \frac{E^s}{s! \prod_{i=1}^{s} h\nu_i} \tag{2.47}$$

$$N(E) = \frac{E^{s-1}}{(s-1)! \prod_{i=1}^{s} h\nu_i} \tag{2.48}$$

where s represents the number of oscillators, E denotes the energy of the activated complex and ν_i is frequency of the oscillator i. The classical expressions for the sum

[b]The active degrees of freedom exchange energy during the reaction, while the adiabatic degrees of freedom remain in the same quantum state during the reaction. The internal degrees of freedom (vibrational and rotational) are considered to be active.

and density of states underestimate the real values of $G(E)$ and $N(E)$ and the use of the equations 2.47 and 2.48 does not provide an accurate description of the chemical process. For the calculation of the RRKM rate constant, the vibrational frequencies and information about the transition state are needed. Nowadays, reliable quantum *ab initio* theoretical calculations can provide these requirements.

In order to apply the RRK and RRKM theory to a particular system and make a comparison with the experimental data, the energy E of the activated complex must be calculated. The approach presented by Cox *et al.*[52] gives a good approximation for E and will be used for the calculation of all RRK and RRKM rate constants presented in this work. The proposed expression for the energy E of the activated complex can be written as:

$$E = E_0 + E_{vib} + E_{free} \tag{2.49}$$

where E_0 is the binding energy of the complex, E_{vib} represents the vibrational energy of the reactants before the reaction and E_{free} is the amount of energy (translational and rotational) of the reactants which is converted into internal energy of the activated complex.

In the case of cluster ion-molecule reactions, the reactant molecules are considered to be vibrationally cold and only the vibrational levels of the ionic clusters are populated. Due to this, E_{vib} represents the vibrational energy of the cluster ion prior to reaction. E_{free} is calculated as the energy difference between the total number

n	$\mathbf{E_{vib}}$	$\mathbf{E_{free}}$	**E**
$n \geq 3$	$(3n-6)k_BT$ (*)	$5/2k_BT$	$E_0 + (3n-7/2)k_BT$
$n \geq 2$	$(3n-5)k_BT$ (**)	$2k_BT$	$E_0 + (3n-3)k_BT$
1	0	$3/2k_BT$ (*)	$E_0 + 3/2k_BT$
1	0	$1k_BT$ (**)	$E_0 + k_BT$

Table 2.1: The vibrational energy E_{vib}, free energy E_{free} and the energy of the activated complex E according to the model proposed by Cox *et al.*[52] n denotes the number of atoms contained in the molecular complex. (*) represents the case of a molecular complex with non-linear geometry, while (**) represents the case of a molecular complex with a linear geometry.

of translational and rotational degrees of freedom for the reactant molecules and the number of the translational and rotational degrees of freedom in the activated complex. A general overview for the values of the vibrational energy E_{vib}, free energy E_{free} and the energy of the activated complex E according to the model proposed by Cox *et al.*[52] for molecular complexes with linear and non-linear structure is given in table 2.1. This model will be applied in chapter 5 to the calculation of the reaction rate constants and binding energies of adsorbed molecules on clusters.

2.3 Cluster Catalysis

In this section, an overview of the catalytic properties of clusters will be presented. First, the general concepts of catalysis will be outlined, including the most important properties of industrial catalysts. After this, the focus will be set on the field of cluster catalysis by discussing the elementary aspects of nanocatalysts and the specific characteristics of clusters, which make them well suited model systems for the study of heterogeneous catalysis. Particular properties of clusters like quantum size effects, structural dynamic fluxionality and isomeric forms will be outlined. A special emphasis will be put on gold clusters and gold nanoparticles, since in the past decade, it was found that nanoscale gold shows surprising catalytic properties. The catalytic behavior of nanoscale gold is significant for current and future applications in the field of chemical and biological sensors, imaging of cells and biomolecules, material science, chemical industry as well as environmental protection and maintenance.[2,6]

2.3.1 Introduction to Catalysis

In 1835, J. Berzelius formulated the first definition of a catalyst as a substance that allows for chemical reactions which would normally not take place, to occur merely through the presence of the catalyst.[53] Fifty years later in 1888, W. Ostwald showed that catalysts influence the reaction rate but do not change the equilibrium state of the chemical reaction.[54] For his pioneering work in the field of catalysis, W. Ostwald received the Nobel prize for chemistry in 1909.

Schematically, a catalyzed reaction between the reactants A and B can be written

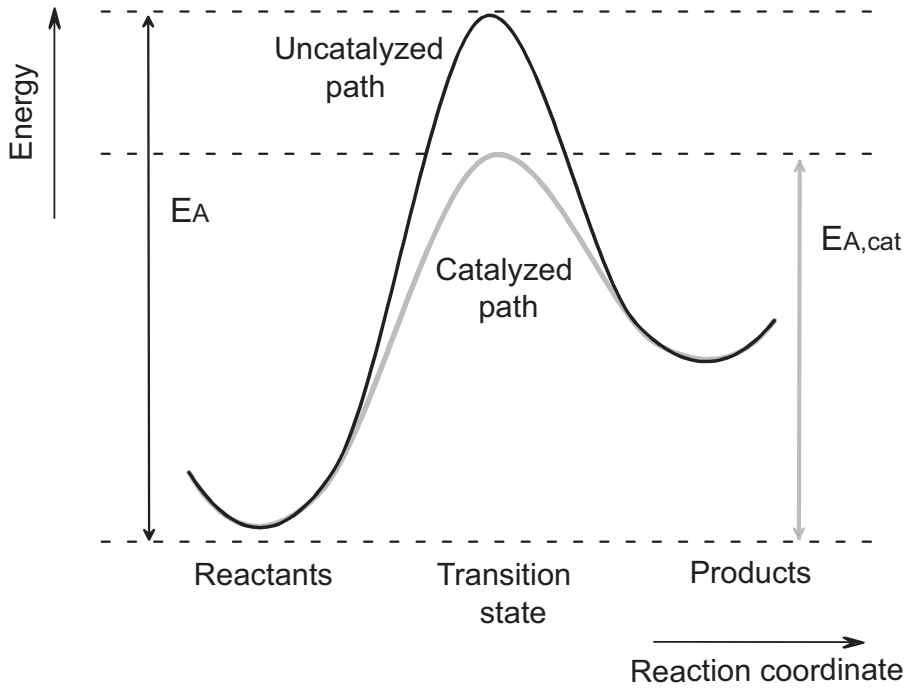

Figure 2.3: The reaction path and the activation energy for a catalyzed (grey line) and an uncatalyzed (black line) chemical reaction. The activation energy for the catalyzed reaction path ($E_{A,cat}$) is considerably lower than the activation energy for the uncatalyzed reaction path (E_A).

as:

$$A + C \rightarrow AC \tag{2.50}$$

$$AC + B \rightarrow AB + C \tag{2.51}$$

where C represents the catalyst. From equations 2.50 and 2.51, it can be seen that the catalyst only enables the chemical reaction to take place and is reformed at the end of a catalytic cycle. The presence of the catalyst leads to a modification of the transition state of the chemical reaction and more specifically, to the lowering of the activation energy barrier. The influence of a catalyst on a chemical process is shown in Fig. 2.3, where a catalyzed and an uncatalyzed reaction path are presented.

A catalyzed equilibrium reaction between species A and B in the presence of a catalyst C can be written as:

$$A + C \leftrightarrows B + C \qquad k_1,\ k_{-1} \tag{2.52}$$

where k_1 and k_{-1} denote the forward and backward reaction rate, respectively. The equilibrium coefficient K has the following expression:

$$K = \frac{k_1}{k_{-1}} = \frac{[B][C]}{[A][C]} = \frac{[B]}{[A]} \tag{2.53}$$

From equation 2.53, it can be seen that the catalyst C appears in the expression of the reaction rates k_1 and k_{-1}, while the equilibrium coefficient K does not depend on the catalyst C. Thus, the catalyst C produces an increase of the reaction rates, compared to the uncatalyzed process but does not affect the equilibrium of the reaction.

One of the most important properties of the catalysts is their selectivity, *i.e.* their ability to favorize one specific reaction channel over another. One example, for which this behavior can be clearly seen is the reaction of carbon monoxide with hydrogen. For this reaction, different products can be obtained (methane, methanol and saturated hydrocarbons) depending on the type of catalyst that is used. Schematically, this process can be written as:

$$\nearrow \quad CH_4 \qquad \mathbf{Ni} \tag{2.54}$$

$$CO + H_2 \longrightarrow \quad CH_3OH \qquad \mathbf{CuO}, \mathbf{Cr_2O_3} \tag{2.55}$$

$$\searrow \quad C_nH_{2n+2} \qquad \mathbf{Fe}, \mathbf{Co} \tag{2.56}$$

where **Ni**, **CuO**, $\mathbf{Cr_2O_3}$, **Fe**, **Co** represent the catalysts used for steering the reaction to the different reaction channels.[55]

When the catalyst and the reactants are in the same aggregation phase (liquid, gas or solid) a *homogeneous catalysis* takes place. When the catalyst and the reactants are in different aggregation phase (liquid-solid, gas-solid), the process is referred to as *heterogeneous catalysis*. Since the chemical process takes place on the interface between gases (or liquids) and solids, this type of catalysis is also known as *interface or surface catalysis*.

In the case of heterogeneous catalysis of a bimolecular reaction, one can distinguish two mechanisms for the reaction to take place:[56]

- the *Langmuir-Hinshelwood mechanism*, where both reactant molecules are preadsorbed on the surface of the catalyst and the reaction occurs by encounters of the adsorbed species, which migrate on the surface. If one considers the two reactant molecules A and B, which are adsorbed on a surface, this mechanism

can be schematically described as:

$$A_{gas} \longrightarrow A_{ad} \tag{2.57}$$

$$B_{gas} \longrightarrow B_{ad} \tag{2.58}$$

$$A_{ad} + B_{ad} \longrightarrow (AB)_{ad} \longrightarrow (AB)_{gas} \tag{2.59}$$

where expression 2.57 describes the adsorption of molecule A on the surface, expression 2.58 shows the adsorption of molecule B on the surface and expression 2.59 describes the encounter, the reaction of molecules A_{ad} and B_{ad} as well as the subsequent desorption of the reaction product (AB). The rate of product formation for this type of reaction is then directly proportional to the surface coverage for molecules A_{ad} and B_{ad}, *i.e.* to the concentration of the adsorbed species.

- the *Eley-Rideal mechanism* in which only one of the reactant molecules is adsorbed on the surface of the catalyst. In this case, the chemical reaction takes place when a gas-phase molecule (the second reactant molecule) collides directly with the molecule which is already adsorbed on the surface. The Eley-Rideal mechanism can be schematically written as:

$$A_{gas} \longrightarrow A_{ad} \tag{2.60}$$

$$A_{ad} + B_{gas} \longrightarrow (AB)_{ad} \longrightarrow (AB)_{gas} \tag{2.61}$$

where expression 2.60 describes the adsorption of molecule A on the surface. Expression 2.61 describes the reaction between the adsorbed molecule A_{ad} and the gas-phase molecule B_{gas} as well as the desorption of the reaction product (AB). In this case, the rate of product formation depends on the surface coverage for molecule A_{ad} as well as on the partial pressure of gas-phase molecules B_{gas}.

The Langmuir-Hinshelwood and Eley-Rideal mechanisms for heterogenous catalysis are applied in the theoretical modelling of reactivity and catalytic properties of deposited clusters on surfaces, as well as in the case of free gas-phase clusters.[10,57]

2.3.2 Nanocatalysis

The catalysts used in industrial processes are usually composed of small metal particles dispersed on a porous material substrate. A well known example is the three-way catalyst (TWC) for cleaning toxic automobile gas emissions. The automotive converter nowadays installed in virtually every new car consists of a honeycomb ceramic substrate covered with porous aluminium oxide, which is impregnated with nanoparticles of platinum, rhodium, ceria, zirconia, lanthana and baria. The role of platinum is to oxidize the unburnt hydrocarbons and carbon monoxide while rhodium is used to reduce the nitric oxides.[58] The importance of small particles in the catalytic processes has stimulated extensive efforts towards their characterization, in order to be able to design new types of catalysts with higher efficiency and selectivity as well as catalysts for new technical applications.

Since the intrinsic mechanisms of the heterogeneous catalysis at the atomic and molecular level are still unknown, model systems have been searched for, which have similar properties to the real catalysts and at the same time, are simple enough to be theoretically described. The development of modern experimental techniques has permitted the production of model systems for the investigation of the mechanisms of heterogeneous catalysis. Deposited nanoparticles and clusters on surfaces as well as gas-phase clusters are considered to be appropriate systems for modelling the elementary reaction steps of heterogeneous catalysis, providing important information for the understanding of the high complexity of real catalysts.

The uniqueness of clusters and nanoparticles consists in their completely different physical and chemical properties in comparison to the bulk materials. During the last decades, it was shown that clusters and nanoparticles possess unexpected catalytic properties.[6,59,60] An important issue in the field of nanocatalysis is whether the geometrical or the electronic structure is responsible for the appearance of size effects in the catalytic properties of clusters and nanoparticles. It was found that in the case of large nanoparticles consisting of more than one hundred atoms, the geometrical structure plays a significant role. For these large nanoparticles, the electronic structure already shows a bulk-like behavior and the number of steps and kinks on the nanoparticle surface as well as the type of crystalline facets determine the catalytic properties.[60,61] In the case of clusters and small nanoparticles that contain several atoms to a few tens of atoms, the catalytic properties are strongly influenced by the

electronic structure. With respect to this, clusters and small nanoparticles show a particular behavior which will be illustrated in the following:[10,62]

- *Quantum-size effects*: for small particles, the electronic structure still has a discrete, quantified character and thus, every cluster with a specific number of atoms and electrons has its own intrinsic characteristic electronic structure which leads to size specific chemical and physical properties. Therefore, by adding or removing a single atom from a cluster, drastic changes in the physical and chemical properties can be obtained. In the case of supported clusters, the interaction between the substrate and the clusters depends on the cluster size as well. This interaction can induce a charge transfer between the clusters and surface, which has a significant influence on the catalytic properties of the supported clusters, as will be shown later. The presence of quantum-size effects opens the perspective of tuning the catalytic properties of clusters and small nanoparticles by changing the cluster size.

- *Structural dynamic fluxionality*: clusters usually possess different isomers which can be energetically close to one another, so that during a chemical reaction an isomerization of the cluster can take place. A change in the geometry of the cluster can lower the activation energy of the desired reaction. Moreover, different isomers may have different reactivities and thus, the selectivity of a chemical reaction can be tuned. This was experimentally observed by Bérces *et al.* through the investigation of the reactivity of gas-phase niobium clusters (Nb_n, $n = 2 - 20$) with H_2 and N_2 at different temperatures.[26] The authors associate the biexponential decrease of the cluster signal as a function of the reaction time with the presence of different isomers with distinct reactivities.[26]

- *Formation of alloy clusters*: when an atom of a different chemical element is introduced in a small particle, the electronic structure of the entire cluster can be changed. The change in the electronic structure leads to a change in the physical and chemical properties of the cluster. Therefore, mixed clusters show completely different physical and chemical properties in comparison to the initial pure clusters, as will be shown in section 5.6.

These special properties of clusters and small nanoparticles open fascinating per-

spectives for creating catalysts with high efficiency and selectivity for specific industrial applications.

In the following, the discussion will focus on the catalytic properties of noble metal clusters and nanoparticles with an emphasis on the catalytic properties of gold towards the carbon monoxide (CO) oxidation reaction. Gold has long been known to be catalytically inactive in contrast to other noble metals like platinum, palladium and rhodium.[63,64] Recently, it was found that deposited gold nanoparticles on metal oxide surfaces show a surprisingly high catalytic activity for low-temperature CO combustion, partial oxidation of hydrocarbons, hydrogenation of carbon oxides and reduction of nitrogen oxides.[6,65] The catalytic properties of gold nanoparticles depend on the particle size, the type of support and the preparation methods of the nanoparticles.

In Fig. 2.4, different possible mechanisms, which aim to explain the unexpectedly high catalytic activity of gold nanoparticles towards CO oxidation, are shown. One of the mechanisms proposes that the adsorption of the reactant molecules occurs on the perimetric atoms of the nanoparticles, where the interaction with the substrate is strong and the number of the active sites (perimetric atoms) increases with the size of the nanoparticle.[6]

A second proposed mechanism assumes that the adsorption of the reactant molecules occurs on the lateral sides of the clusters ("sticky sides"), especially on the edge atoms, which have a smaller coordination number than the atoms on the top side.[1] In order to quantitatively characterize the ability of deposited nanoparticles to catalyze a chemical reaction, the turn-over frequency is defined as:

$$TOF = \frac{Number\ of\ product\ molecules}{Number\ of\ active\ sites\ \cdot second} \tag{2.62}$$

In expression 2.62, the active sites represent the positions where the reactant molecules are adsorbed (perimeter atoms, edge atoms etc.). These two mechanisms illustrate the influence of geometrical effects on the catalytic properties of large nanoparticles as discussed above.

By reducing the size of the gold particles, a different mechanism for the catalytic CO oxidation is observed. Valden *et al.* deposited small gold nanoparticles with a diameter between 2 nm and 4 nm (two-atomic-layer thick particles), on titanium dioxide $TiO_2(110)$ thin films and observed that these particles exhibit an unusually

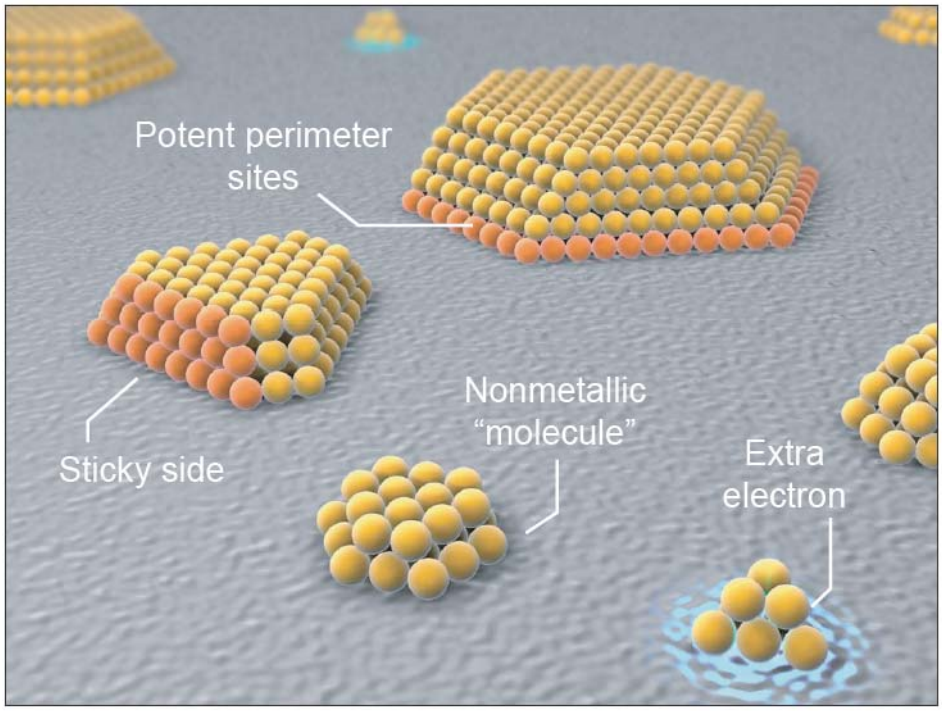

Figure 2.4: Possible mechanisms for catalytic CO oxidation reaction *via* deposited gold nanoparticles and clusters, taken from Cho *et al.*[1] The reactant molecules adsorb preferentially on "sticky" sides and perimeter sites. When the nanoparticle size decreases, it becomes nonmetallic. A charge transfer between surface and cluster can occur when the particle contains only a few atoms.

high catalytic activity towards the CO oxidation reaction.[66] The authors correlate the unexpected catalytic activity with a quantum-size effect, *i.e.* with the appearance of the nonmetallic character of the small gold nanoparticles in this size range. This is illustrated in the opening of a band gap of $0.2\ eV - 0.6\ eV$ that does not exist in bulk gold metal.[66]

As shown in Fig. 2.4, when the size of the gold particles is further reduced to a few atoms or a few tens of atoms, another mechanism for the catalytic activity appears. This mechanism involves a charge transfer between the surface and the deposited gold clusters. The experiments performed by Sanchez *et al.*, in which mass-selected gold clusters (Au_n, $n \leq 20$) were deposited on a thin film of magnesium oxide $MgO(100)$, showed that gold clusters which contain at least eight atoms (Au_8) enable the oxidation reaction of carbon monoxide to carbon dioxide.[10] In Fig. 2.5, the number

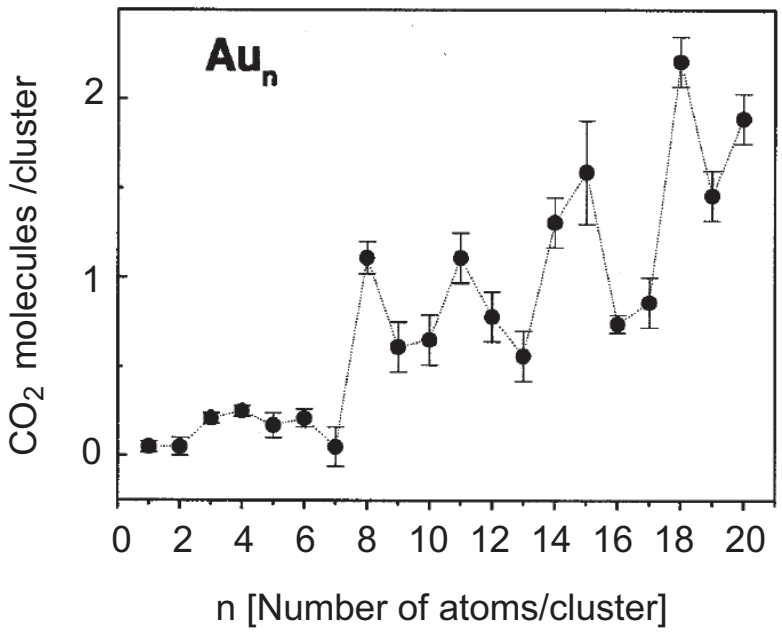

Figure 2.5: The CO oxidation reaction enabled by small gold clusters deposited on a thin film of magnesium oxide, taken from Sanchez *et al.*[10] The carbon dioxide yield is depicted as a function of the cluster size.

of CO_2 molecules produced per cluster is depicted as a function of cluster size. From this figure, it can be seen that every cluster size shows a distinctly different reactivity towards the oxidation of carbon monoxide. Gold clusters which contain less than eight atoms (Au_n, $n < 8$) do not promote the oxidation of CO, while gold clusters with more than eight atoms (Au_n, $n \geq 8$) yield between one and two CO_2 molecules per cluster. It was also observed experimentally that the quality of the $MgO(100)$ thin film, *i.e* the density of defects influence the efficiency of the oxidation reaction. The defects consist mainly of oxygen-vacancy F-centers, where the charge density is higher. The experiments showed that when clusters are deposited on defect-rich MgO thin films, the yield of produced carbon dioxide is higher than in the case of defect-poor MgO thin films.[10]

The theoretical calculations performed by H. Häkkinen and U. Landman elucidated the mechanism of the chemical reaction at molecular level and revealed that a charge transfer between the MgO surface and cluster occurs, loosening the oxygen-oxygen bond and thus making the CO oxidation reaction possible.[10] Moreover, the

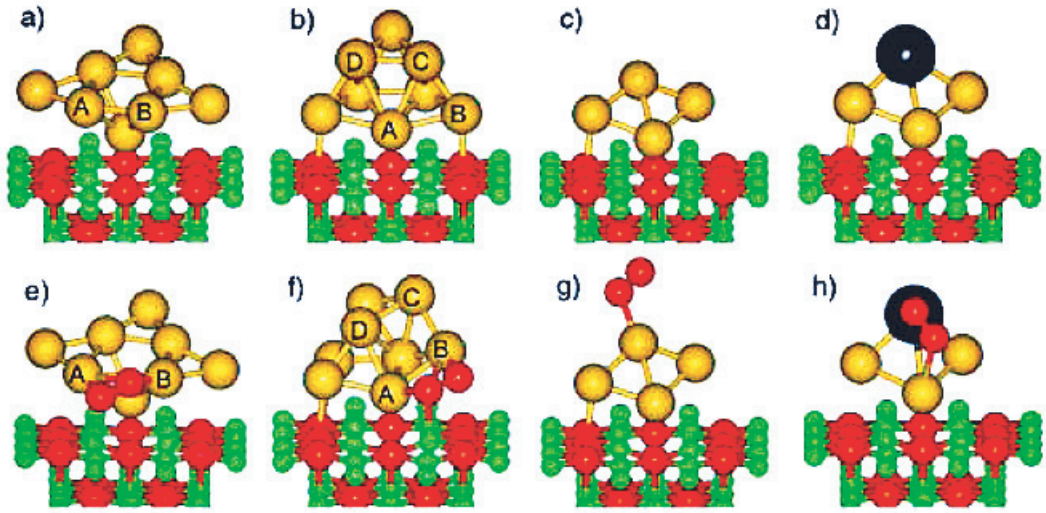

Figure 2.6: The structure of bare gold and mixed gold-strontium clusters deposited on MgO thin films. (a) and (b) Au_8, (c) Au_4, (d) Au_3Sr, (e) and (f) Au_8O_2, (g) Au_4O_2, (h) Au_3SrO_2, taken from Häkkinen *et al.*[62]

charge transfer between magnesium oxide surface and gold cluster depends on the cluster size. It was found that in the case of Au_8, the charge transfer amounts 0.5 e, where e represents the elementary charge, while in the case of Au_4 clusters the charge transfer has a value of only 0.3 e. The theoretical calculations also predicted that the binding energy of Au_8 clusters on F-centers is about 2 eV higher than on defect-free MgO thin films.[10] In conclusion, it was shown that the charge transfer between the deposited gold clusters and the magnesium oxide substrate plays a decisive role in the CO oxidation reaction on small gold clusters. This combined experimental and theoretical work represents an outstanding example for the significant role of quantum-size effects in the catalytic properties of gold clusters. From the theoretical simulations for the catalytic oxidation of carbon monoxide by Au_8 clusters deposited on magnesium oxide thin films, it was further observed that the structure of the Au_8 clusters changes from an octahedral (Fig. 2.6 (b)) to a trigonal-prismatic structure (Fig. 2.6 (f)), when an oxygen molecule is adsorbed. This structural fluxionality of Au_8 clusters is necessary for the catalytic process, since the adsorption and activation of the oxygen molecule (the loosening of the $O-O$ bond) would not be possible without this isomerization.[62]

The experimental investigation of the catalytic properties towards CO oxidation of mixed gold-strontium clusters (Au_nSr, $n \leq 9$) deposited on magnesia thin films revealed that the first catalytically active cluster is Au_3Sr_1 and the CO_2 yield is higher than in the case of pure gold clusters.[62] The structure of Au_3Sr clusters, before and after the adsorption of the oxygen molecule is presented in Fig. 2.6 (d) and (h). The presence of a strontium atom embedded into pure gold clusters reduces the minimum number of gold atoms, which are necessary to start the CO oxidation reaction, from eight to three. In this way, the formation of alloy clusters has a decisive influence on the catalytic properties.

In order to gain a better understanding of the underlying mechanisms of heterogeneous catalysis, charged clusters in the gas-phase are well suited as model systems. The advantage of gas-phase clusters is that the interaction with a substrate, which is difficult to treat in theoretical calculations, is eliminated and that a full charge (positive or negative) is available on the clusters. Furthermore, the presence of a charge on the clusters allows the simulation of the charge transfer which occurs in the case of deposited clusters on surfaces.

The first catalytic cycle in the gas-phase with cationic iron atoms Fe^+ as catalysts was reported by Kappes *et al.*[67] for the chemical reaction:

$$N_2O + CO \rightarrow CO_2 + N_2 \tag{2.63}$$

For the catalytic oxidation reaction of carbon monoxide:

$$CO + O_2 \rightarrow CO_2 + 1/2O_2 \tag{2.64}$$

the first full thermal catalytic cycle in the gas-phase, carried out by small platinum clusters (Pt_n^-, $n = 3 - 6$) was experimentally observed by Shi *et al.*[25] A full thermal cycle represents a cyclic reaction in which bare metal clusters react with molecules, the reaction products are desorbed and, in a last step, the bare metal clusters are reformed and start another cycle. All mentioned processes are carried out at thermal energies. The experiments were performed by using a flow tube reactor, where bare platinum clusters react with oxygen and $Pt_nO_m^-$ products are obtained, with $m = 1, 2$. These products are then mass-selected and further transferred inside a radio frequency octopole ion beam guide, where the reaction with CO takes place. The final reaction products are detected by using a quadrupole mass spectrometer.[25] The schematic

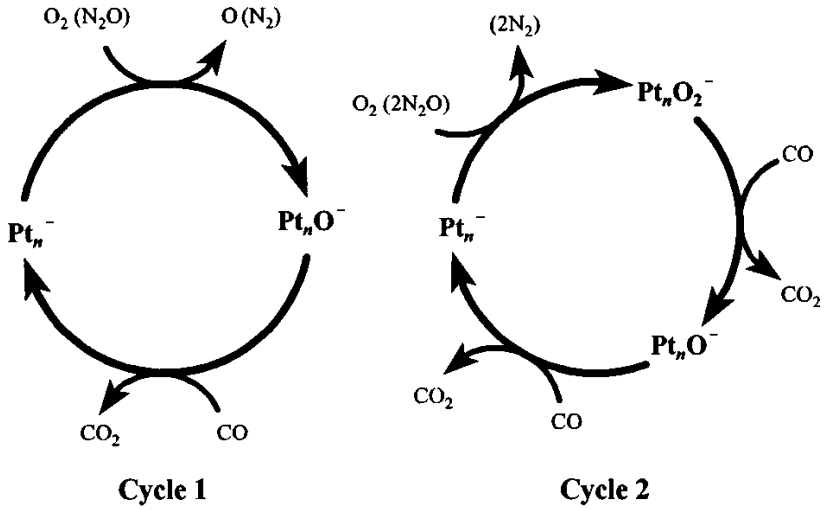

Figure 2.7: The catalytic cycles for the *CO* oxidation reaction *via* small, negatively charged platinum clusters, taken from Shi *et al.*[25]

representation of the catalytic cycle is shown in Fig. 2.7. Two reaction paths for the catalytic oxidation of carbon monoxide have been identified: one pathway involves the formation of Pt_nO^- as an intermediate product (Fig. 2.7, Cycle 1), while in the other reaction path $Pt_nO_2^-$ and Pt_nO^- appear as intermediate complexes (Fig. 2.7, Cycle 2).

As will be shown in chapter 5, the reactivity of small, negatively charged noble metal clusters towards oxygen and carbon monoxide in the gas-phase shows pronounced quantum size effects, *i.e.* by adding or removing a single gold atom the reactivity changes drastically. Moreover, it will be shown that the charge and the chemical composition of the clusters strongly influence their chemical reactivity.

In conclusion, there are two relevant size-ranges in the reactivity of nanoparticles and clusters. For large nanoparticles which contain hundreds of atoms, the geometric effects (steps, edges, kinks) determine the catalytic properties. For the small nanoparticles and clusters, which contain between a few atoms and a few tens of atoms, the electronic structure plays an significant role, which leads to a pronounced size-dependent catalytic activity, where each atom counts.